



# Impact of Cr nanocrystalline discrete crystal nuclei on demolding strength and surface roughness of precision electroforming Ni layer on Cu substrate

Guang Yang<sup>1</sup> · Ju Chen<sup>1</sup> · Bo Li<sup>1</sup> · Qinfeng Wang<sup>1</sup> · Yuzhou Zhang<sup>1</sup> · Jun Pi<sup>1</sup>

Received: 18 December 2021 / Accepted: 26 March 2022 / Published online: 10 April 2022  
© The Author(s), under exclusive licence to Springer Nature B.V. 2022

## Abstract

The demolding quality of the electroforming Ni layer on Cu mold determines the machining accuracy of high-end optical mold. Although the fabrication of an anti-adhesion layer with controllable demolding strength is paramount, it remains quite challenging. Herein, we report a one-pot strategy to electrodeposit Cr nanocrystalline discrete crystal nuclei through electrochemical deposition from trivalent Cr salt. The nucleation characteristics of the Cr element were described. Cr nanocrystalline discrete crystal nuclei change the lattice constant of the electroforming Ni layer. In addition, XPS results show that Cr nuclei form oxides on Cu substrates, the passivation layer leads to a significant decrease in the interface bonding force and the surface roughness of the electroforming Ni layer after demolding. The test results show that the demolding strength and surface roughness  $R_a$  are the least when the density of Cr crystal nuclei is  $10.85 \times 10^{11} \text{ cm}^{-2}$ . Notably, the Cr nanocrystalline discrete crystal nuclei are simple to prepare, controllable for demolding strength, non-toxic, and exhibit great potential as an anti-adhesion layer.

---

✉ Guang Yang  
yangg@jmu.edu.cn

Ju Chen  
1615737342@qq.com

Bo Li  
200661000155@jmu.edu.cn

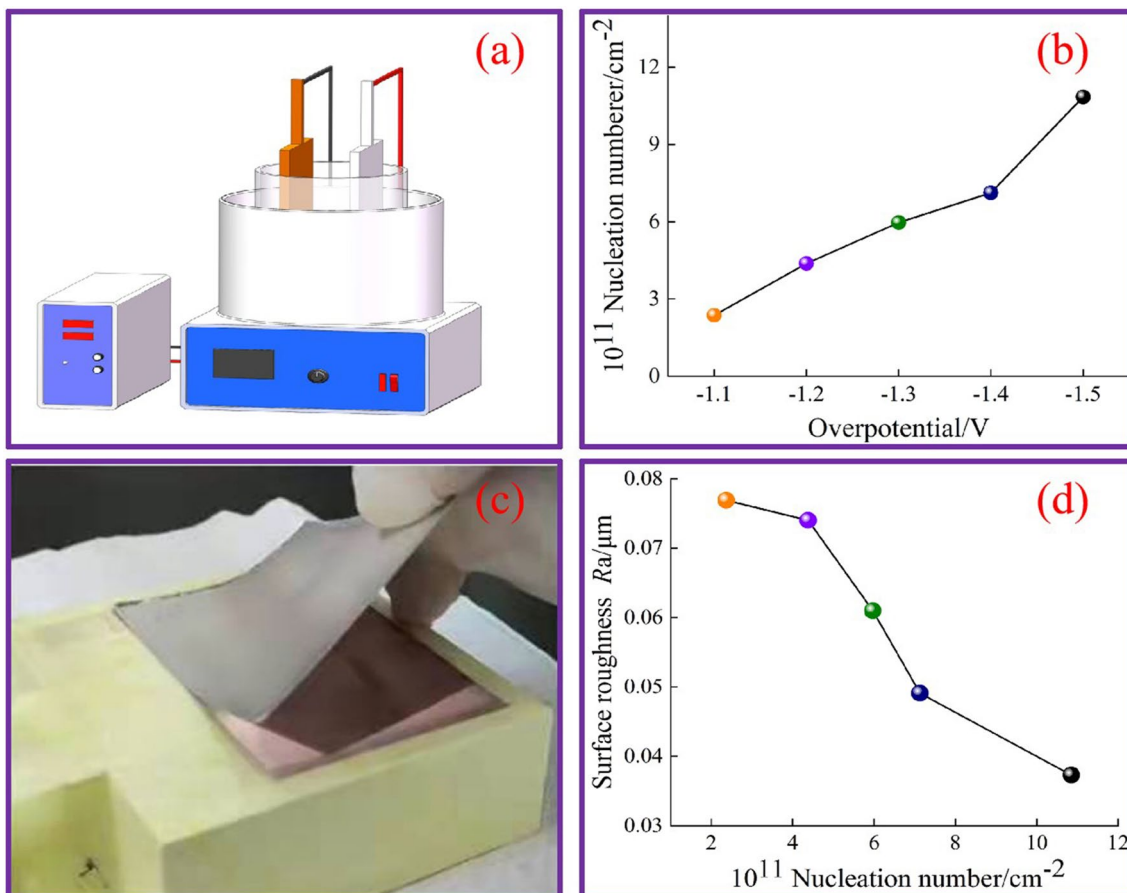
Qinfeng Wang  
200561000092@jmu.edu.cn

Yuzhou Zhang  
199461000016@jmu.edu.cn

Jun Pi  
pi\_jun@163.com

<sup>1</sup> College of Marine Equipment and Mechanical Engineering, Jimei University, 9 Shigu Rd., Jimei District, Xiamen 361021, Fujian, People's Republic of China

## Graphical abstract



**Keywords** Optical mold · Electroforming · Demolding strength · Surface roughness · Chromium nucleation

## 1 Introduction

In recent years, with the rapid development of new energy and energy-saving technology, new media, and information technology, there has been an increased demand for high-end microstructure optical thin-film materials. The shape accuracy and surface roughness of the working dye of the high-end optical film are measured by reflectivity as  $R_a < \lambda/100$  ( $\lambda$  is the wavelength of visible light) [1–3]. Therefore, surface roughness and shape position error of the microstructure are below tens of nanometers [4, 5]. The electroforming error of the microstructure optical mold is mainly caused by plastic deformation. The surface modification of the original mold can reduce the plastic deformation of the demolding, which is closely related to the control of interface bonding strength. However, the bonding strength between the electrolytic Cu substrate and the electroforming Ni layer involves several physical and chemical factors and understanding the mechanism by

which the anti-adhesion layer regulates the bonding force remains a challenge.

The anti-adhesive layer is an effective means to control the interface bonding force. Potassium dichromate solution is used for demolding in the industry; however, it is a carcinogenic chemical, and its coating cannot regulate the bonding force between the substrate and the casting layer, resulting in an unstable demolding effect [6, 7]. Analyses of various tests of non-potassium dichromate have found no connection between the thickness of the anti-adhesion layer and the demolding accuracy [8, 9]. The thickness and continuity of the anti-adhesion layer are unknown, and the relationship between demolding-induced plastic deformation and macroscopic mechanical properties of the interface is unclear. Therefore, the test results are difficult to be applied in precision electroforming. These factors limit our ability to prepare anti-adhesion layers and understand the mechanisms by which they regulate interface bonding force [10].

Herein, we develop a precise electroforming-assisted demolding strategy using Cr nanocrystalline discrete crystal nuclei for electroforming Ni layer on Cu substrate. First, fine Cr discrete crystal nuclei were prepared on Cu substrates by direct current deposition. Then, a Ni layer was electroformed on the Cu substrates. The use of Cr discrete crystal nuclei reduces the bonding force between the Cu substrate and the deposited Ni layer, which is consistent with the report of Hidekazu. The crystal structure of the substrate and the casting layer were characterized by X-ray diffraction (XRD) measurements [6]. The results demonstrate that the crystal nuclei of Cr lead to the change of the lattice constant of the Ni deposition layer. The lattice distortion of Ni is closely related to the density of Cr discrete crystal nuclei, and their law is discussed. Moreover, molecular dynamics calculations show that Cr oxides can reduce the bonding force between the substrate and the electroforming layer. The binding force between the Cu/Ni and the surface roughness of the Ni electroforming layer is controlled by the density of Cr crystal nuclei.

## 2 Experimental details

### 2.1 Fabrication of Cr nanocrystalline discrete crystal nuclei

First, a Cu sheet with an area of approximately  $5 \times 6$  cm was ground and polished to a sub-micron roughness. The electrode was soaked in acetone for 5 min to remove oil and in acetic acid for 1 min to remove the oxide layer and then put in an ultrasonic cleaning device for 10 min. It was then rinsed with pure water, dried with nitrogen, and pasted on the cathode plate. Areas were insulated except for electroplating and then it was put into the electrolytic cell of the trivalent Cr solution system for electrodeposition. The bath compositions and Cr crystal nuclei electrodeposition are as follows: chromium sulfate hydrate ( $25 \text{ g L}^{-1}$ ), ammonium chloride ( $250 \text{ g L}^{-1}$ ), boric acid ( $60 \text{ g L}^{-1}$ , analytically pure), and glycine ( $30 \text{ g L}^{-1}$ ). The electrodeposition temperature was kept at  $43^\circ\text{C}$ . Boric acid as a buffer,  $60 \text{ g L}^{-1}$  dosage can ensure the system pH value between 3.0 and 3.5 in the electroplating process [11]. Lower temperature affects the deposition rate. Higher temperatures will weaken the cathodic polarization of Cr ions and lead to a stronger hydrogen evolution reaction, reducing the current efficiency [12]. Through experiments, the optimal control temperature is  $43^\circ\text{C}$ . The time of electrodeposition was determined by observing the time–current curve: when the current value reached the highest, the deposition of Cr discrete crystal nuclei was completed.

### 2.2 Fabrication of electroforming Ni layer

First, the electroforming solution was prepared according to the proportion of nickel sulfamate ( $150 \text{ g L}^{-1}$ ), nickel chloride ( $150 \text{ g L}^{-1}$ ), and chloride ion ( $150 \text{ g L}^{-1}$ ). The pH value of the electroplating solution was 3.5–4.0. Then, the Cu substrate with Cr discrete core deposited on the surface was placed vertically in the plating tank as the cathode, and the pure Ni plate was placed parallel to the cathode as the anode, with a spacing of 8 cm. After 3.5 h under the current density of  $4 \text{ A dm}^{-2}$ , the Cu substrate was removed and washed with deionized water. Finally, Ni deposition layers were carefully separated from their Cu substrates and washed with deionized water. Electroforming Ni mold is used as the working mold in the production process of the optical film and its thickness should meet requirements of 0.5 mm. The required electroplating thickness can be achieved in 3.5 h under the current density of  $4 \text{ A dm}^{-2}$ .

### 2.3 Characterization

Electrochemical tests were conducted on an electrochemical workstation (CHI660E, Shanghai, China) with a three-electrode system. A Pt slice was used as the counter electrode and a saturated calomel electrode (SCE) was used as the reference electrode. The surface roughness  $R_a$  of the electroforming Ni layer was measured using a laser confocal microscope (VK-X1000, Japan). The sample is cleaned using an ultrasonic cleaning device (DSA300-GI.2 China). During measurement, appropriate magnification was selected, three positions were chosen on the surface of each nickel sheet, and roughness measurements were made along three different directions at each point. The average value was calculated as the surface roughness value of the point. The surface morphology and surface chemical elements of Cr discrete crystal nuclei and nickel coating were analyzed using a plenum-XL scanning electron microscope (15 kV UHV secondary electron method, Japan) and Sigma 500 field emission scanning electron microscope (5 kV UHV, In-Lens method, Germany), respectively. The crystal structure of nickel coating was measured by X-ray diffraction (X'Pert Pro, 40 kV working voltage, 30 mA current, the Netherlands), using Cu  $K\alpha$  line radiation source ( $\lambda = 0.154 \text{ nm}$ ). The range of  $2\theta$  angles was  $5\text{--}85^\circ$  and the diffraction angle scanning speed was  $3^\circ \text{ min}^{-1}$ . XPS spectra were performed using PHI Quantum 2000 (Physical electronics Co., Ltd., USA) system with an Al  $K\alpha$  line source ( $h\nu = 1486.6 \text{ eV}$ ) at an incident angle of  $45^\circ$ . Quantitative surface and interface analyses were conducted using the peak areas of the high-resolution spectra and the Scofield sensitivity factors [13, 14].

### 3 Results and discussion

#### 3.1 Fabrication of Cr nanocrystalline discrete crystal nuclei and electroforming Ni layer

Figure 1 shows the schematic of the preparation of Cr nanocrystalline discrete crystal nuclei and electroforming Ni layer. The Ni layer deposited directly on the surface of the Cu matrix shows good adhesion. A large amount of material transfer occurs on the surface of the Cu matrix and Ni layer, even with forced tearing, which increases the surface roughness of electroforming [15]. Cr crystal nuclei were deposited on the Cu surface. Then, the Ni layer was electroformed to form an ultrathin Cr–Ni zone between Cu/Ni interfaces (Fig. 1b). There, the size is between 17 and 30 nm and the height is about 0.5 nm. The deposited Cr nuclei are easily oxidized and passivated layer is formed on the Cu surface. The passivation layer reduces the bonding force between the Cu substrate and the Ni casting layer, which makes the Ni replica easily separate from the Cu substrate. XPS tests of Cu substrates with deposited Cr nuclei and molecular dynamics calculations of the structure clarify these two points, see Sect. 3.3.

#### 3.2 Nucleation characteristics of Cr discrete crystal nuclei and the influence of its density on demolding strength

To guarantee the accuracy of the film release of precision electroforming, the size of the Cr crystal nuclei should be on the nanometer scale. According to the principle of electrodeposition, the nucleation rate of the crystal during

crystallization of the deposited layer is related to the growth rate of the crystal grain and the parameters of the electroplating system. If the growth of the crystal nuclei formed on the deposited surface is greatly inhibited, ultra-fine crystal grains may be obtained. In addition, the ability of Cr nanocrystalline discrete crystal nuclei to adjust the Cu/Ni interface bonding force is associated with the density of the crystal nuclei [16–19]. Therefore, whether the density of the nano-sized Cr crystal nuclei is controllable is a prerequisite for controlling the release force.

To this end, we explored the nucleation characteristics of trivalent Cr in the system and dynamic parameters of Cr as shown in Fig. 2. First, electrochemical tests were performed using an electrochemical workstation. The working electrode (Cu sheet) with an area of about  $1 \times 3$  cm was ground and polished to a sub-micron roughness. The electrode was soaked in acetone for 5 min to remove oil and in acetic acid for 1 min to remove the oxide layer and then put in an ultrasonic cleaning device for 10 min. It was blow-dried with nitrogen for later use. A three-electrode cell with a counter electrode made of platinum and a saturated calomel electrode (SCE) as the reference electrode was accustomed. Subsequently, deposition potential was performed using the electrochemical workstation, and the step potentials were  $-1.1$ ,  $-1.2$ ,  $-1.3$ ,  $-1.4$ , and  $-1.5$  V. The temperature was  $43^\circ\text{C}$  and the deposition process was monitored by the current versus time ( $i-t$ ) curve [20, 21]. It can be seen from Fig. 2a that the current reached a maximum value within a very short period at the beginning of the experiment, indicating that the Cr element has undergone a typical nucleation process. The current decreases until it stabilizes with the growth of Cr crystal nuclei. In addition, chronoamperometric curves show the characteristics of a typical three-dimensional nucleation curve under diffusion control: as the step potential shifts negatively, the limiting current and steady current in the curve show an increasing trend. The chronoamperometric curves test data are normalized based on  $i^2/i_m^2 - t/t_m$  and compared with the theoretical curve of the Scharifker–Hills (SH) model [22], and the result is shown in Fig. 2b. The normalized experimental curve tended toward the theoretical curve of transient nucleation, indicating that in this system, the nucleation of Cr element electrodeposited on the Cu surface is more in line with the 3D transient nucleation under diffusion control. The nuclear mechanism is consistent with the conclusion of the previous literature. The microscopic morphology of the deposited Cr crystal nuclei is illustrated in Fig. 3. The size is between 17 and 30 nm and the height is about 0.5 nm.

In the case of transient nucleation, the nucleation density gradually increases [the variation range is  $(2.37\text{--}10.85) \times 10^{11} \text{ cm}^{-2}$ ] with the negative shift of the potential, which is consistent with the test results of Song

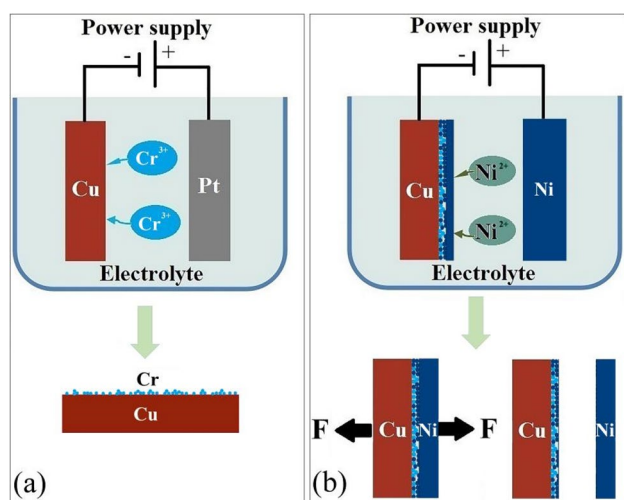


**Fig. 1** Schematic of the preparation of Cr nanocrystalline discrete crystal nuclei and electroforming Ni layer

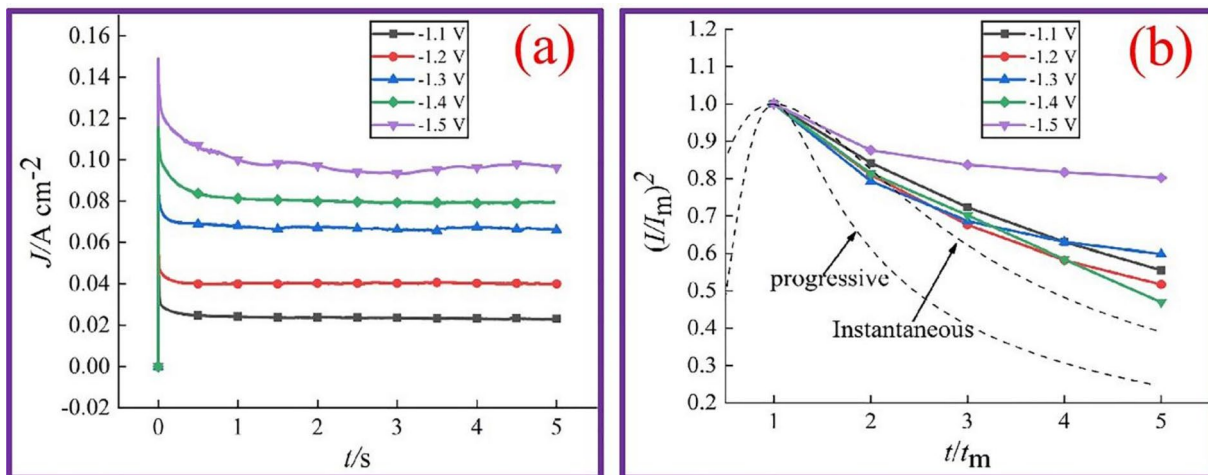


**Fig. 2** Analysis of deposition characteristics of Cr discrete crystal nuclei. **a** Chronoamperometric curves under different step potentials; **b** non-dimensional chronocurrent curve  $i^2/i_m^2-t/t_m$  under different

step potentials ( $i_m$  is the limit diffusion current density,  $t_m$  is the limit diffusion current density time used for current density)

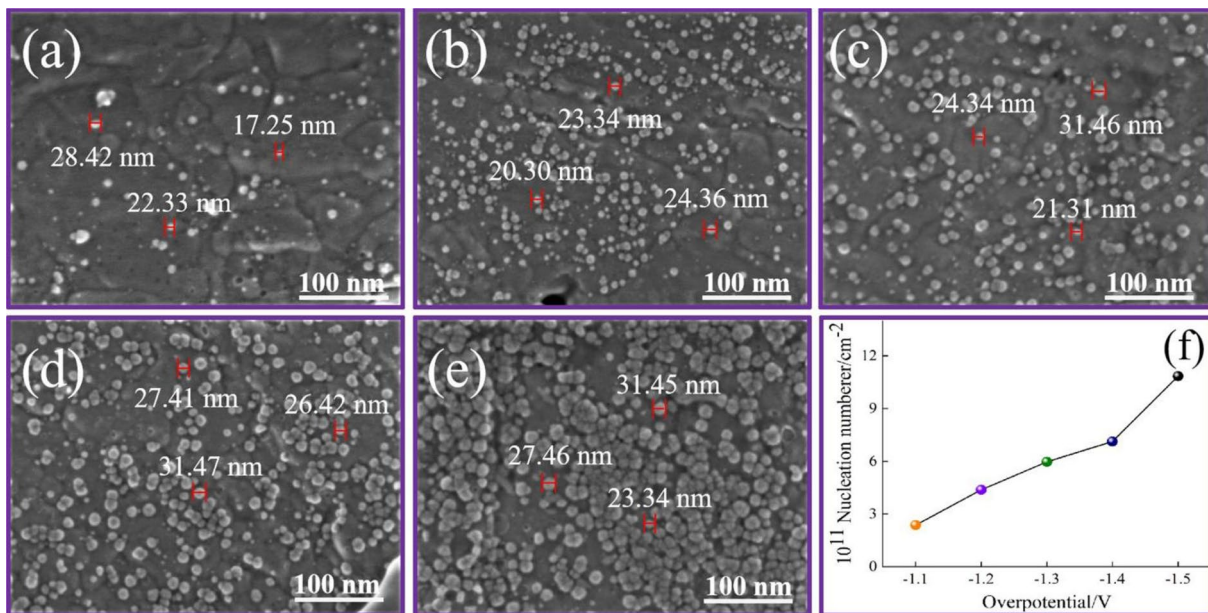


**Fig. 3** **a–e** are, respectively, the microscopic morphology of Cr discrete crystal nuclei deposited under step potential (–1.1, –1.2, –1.3, –1.4, –1.5 V). **f** The number of Cr discrete crystal nuclei

et al. Figure 3f shows the number of nucleation calculated by the test with the change of overpotential [15, 23–25].

The influence of Cr nucleation density on demolding strength was studied, and the results are shown in Fig. 4. It was found that the demolding strength showed decreasing trend with the increase of nucleation density. When the nucleation density is lower than  $7.13 \times 10^{11} \text{ cm}^{-2}$ , the Cu surface modification is weak, and the auxiliary demolding effect is not significant. However, when the nucleation

density is higher than  $7.13 \times 10^{11} \text{ cm}^{-2}$ , as the nucleation density increases, the demolding effect is better.

Hidekazu proposed a electroforming process for the replication of surfaces having nanometer-level smoothness. In the electroforming process, the Cr layer is prepared by electron beam on the substrate and used to separate the substrate from the coating. Research points out that the crucial point in this process is the amount of Cr atoms deposited. By controlling the density of Cr atoms on the master surface, the binding

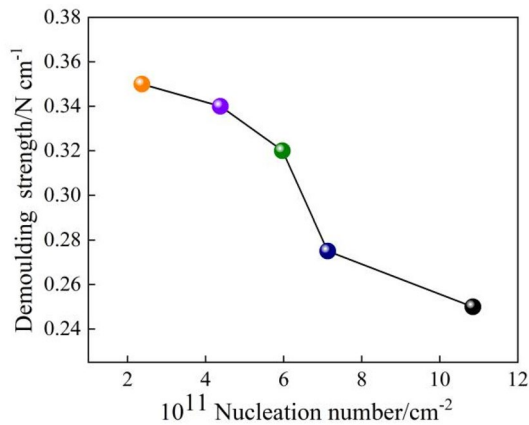
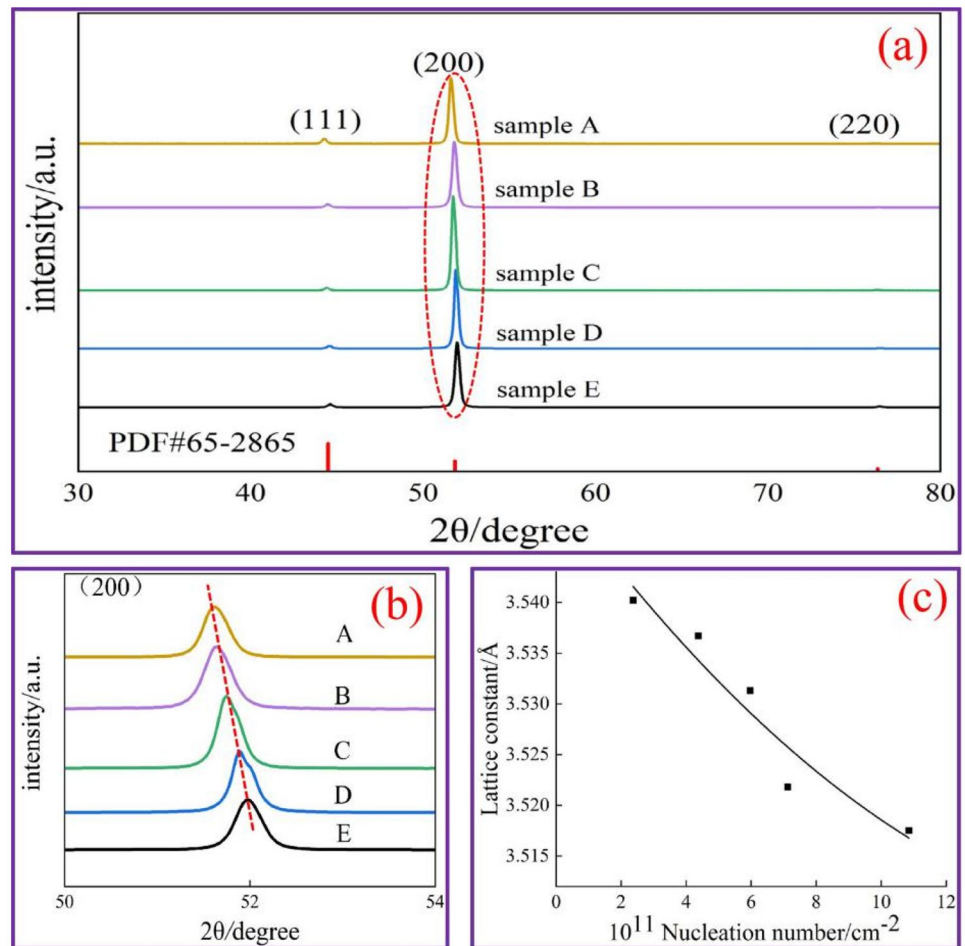


**Fig. 4** Impact of nucleation density on demolding strength

strength between the nickel film and master surface can be adjusted, which makes it possible to separate the metal film from the master surface smoothly [6]. Similar results have been obtained in the demolding experiments with lead nuclei [15].

**Fig. 5** XRD pattern of Ni layer with different densities of Cr crystal nuclei. **a** XRD pattern of Ni layer with different densities of Cr crystal nuclei; **b** XRD enlarged image of Ni texture orientation (200); **c** curve of the lattice constant of electrodeposited Ni layer with different densities



### 3.3 Effect of Cr crystal nuclei density on lattice constant and demolding strength of the deposited Ni layer

The XRD patterns of the plating electroforming Ni layer on the surface of the five-deposited Cr samples are shown in Fig. 5a. Diffraction peaks at  $2\theta = 44.5^\circ$ ,  $51.8^\circ$ , and  $76.4^\circ$  correspond to (111), (200), and (220) crystal planes peak of nickel, respectively. In the electrodeposition process, the crystal orientation of Cu as the substrate is (200) plane. Ni atoms and Cu atoms are mutually soluble. The electrodeposited fresh atoms were incapable of migrating to (111) plane, and some of them would rest on (200) plane, which consequently accelerated the growth of (200) plane and influenced the preferred orientation [26, 27]. As a result, the Ni coating exhibits obvious (200) preferred orientation.

It can be seen that the diffraction peak of the maximum texture, (200) crystal plane peak of electrodeposited Ni near the Cu surface, is shifted under different Cr nucleation densities, indicating that the lattice constant changes (Fig. 5). Most likely, the preference change observed in a shift of the diffraction peak could be attributed to the change in the

lattice constant due to Cr crystal nuclei. (200) diffraction peak intensities are skewed to the right, resulting in a smaller crystal plane distance, indicating that the grain size of Ni decreases [28–31]. Figure 5c reveals that the lattice constant of the electrodeposited Ni layer decreases with the increase of Cr nucleus density. The experiment results showed that when the Cr nuclei were deposited, the lattice constant of Ni layer was reduced by 0.6412% from 3.5402 to 3.5175 Å; and the grain size of the Ni layer was reduced by 68.3% from 268 to 185 nm.

Low interfacial energy and thus a high adhesion are obtained when the structural matching between the substrate and the electrodeposited layer is good. Ni had an fcc structure, and the lattice mismatch between the Ni and Cu was only 2.62%. However, due to the presence of Cr discrete crystal nuclei, the lattice constants of the Ni

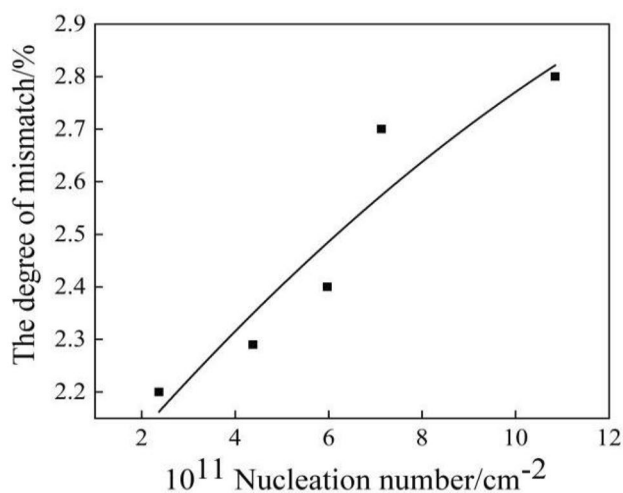


**Fig. 6** Effect of density of Cr discrete nuclei on lattice mismatch between Ni deposition layer and Cu substrate

deposition layer changed, resulting in an increased mismatch between the Ni layer and Cu substrate [32–34], as shown in Fig. 6. The increasing mismatch between the Ni layer and Cu substrate reduces the bonding force between them [35].

Chromium metal is easily passivated. The wide range XPS spectrum of Cu surface with Cr discrete crystal nuclei is shown in Fig. 7a. The XPS test results (Fig. 7b) showed a Cr–O peak appeared and a lower binding energy component occurred, which can be explained by the Cr oxidized species, most probably Cr<sub>2</sub>O<sub>3</sub> [36].

When there are no Cr discrete crystal nuclei between Cu/Ni interface, due to the low strength of the Cu substrate, cracks expand in the Cu matrix until fracture during demolding when the structure is stretched [37–40], as shown in Fig. 8d. We also calculated the strength of the complex using molecular dynamics. Passivation film reduces the interface bonding force. Figures 7d and 8c show corresponding molecular dynamics calculations under two conditions. In Fig. 8c, the number of Cr discrete crystal nuclei on the Cu surface was 45% of that on the paved interface. The results showed that the number of Cu atoms transferred to the side of the electroforming Ni layer was 5686 when there were no Cr discrete crystal nuclei between Cu/Ni interfaces. Due to the presence of Cr discrete crystal nuclei, 141 Cu atoms were transferred to one side of the electroforming Ni layer after demolding. The amount of Cu atom transfer was associated with the density of the Cr discrete crystal nuclei. The number of Cu atoms transferred to the side of the electroforming Ni layer decreases with the increase of the Cr discrete crystal nucleus density. The less the number of transferred Cu atoms, the lower the surface roughness of the electroforming Ni layer. The surface roughness test results of the cast electroforming Ni layer after demolding are further discussed in Sect. 3.4.

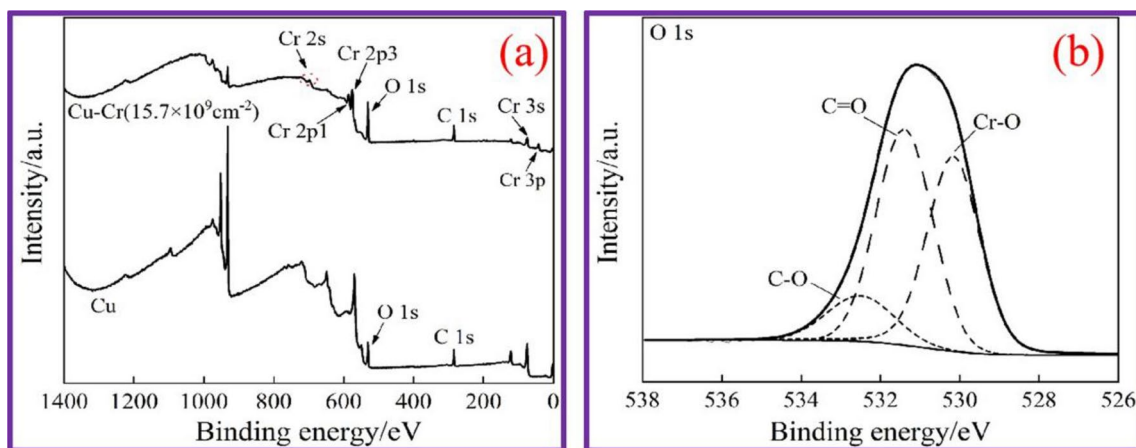


**Fig. 7** **a** The wide range XPS spectrum of Cu surface with Cr discrete crystal nuclei; **b** O 1s spectra and peak fitting

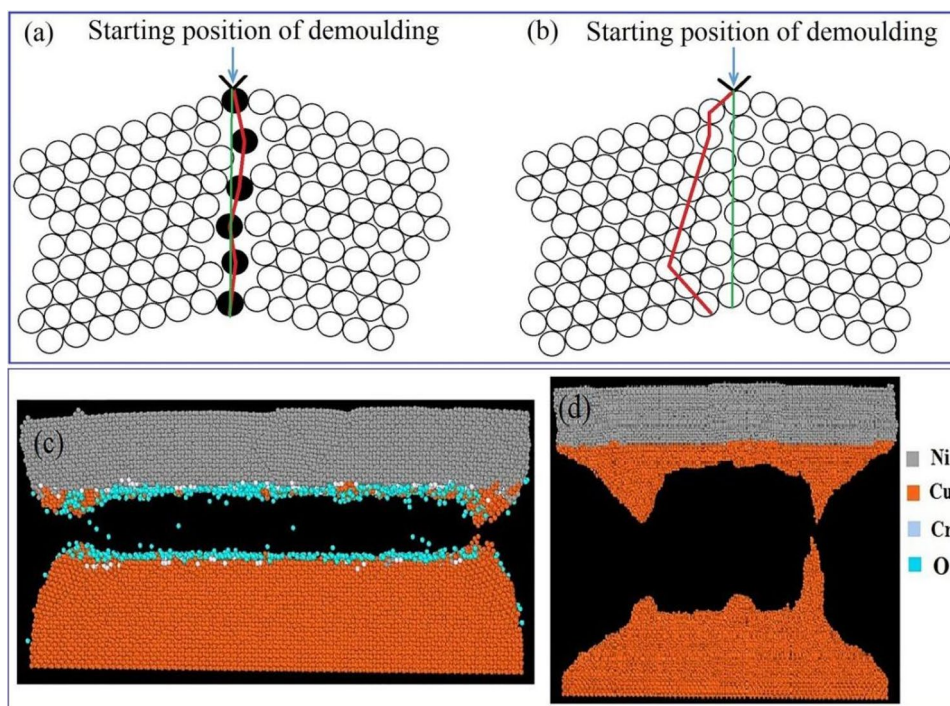


**Fig. 8** Schematic diagram of interface demolding principle and calculations of interface demolding by molecular dynamics. **a** Schematic diagram of interface demolding principle with discrete crystal nuclei and “black dots” represent discrete heterogeneous crystal nuclei introduced artificially and distributed intermittently on the interface. When the release force is applied, the crack extends along the bonding surface (red line) and “ideal tearing” occurs; **b** schematic diagram

of interface demolding principle without discrete crystal nucleus. In absence of discrete heterogeneous crystal nuclei, the crack propagation deviates from the bonding plane (red line) and “non-ideal tearing” occurs (In Fig. 7a and b, the green line represents the interface position.); **c** calculation of interface demolding with Cr discrete crystal nuclei; **d** calculation of interface demolding of Cr-free discrete crystal nuclei. (Color figure online)

### 3.4 Effect of Cr discrete nucleus density on surface roughness

The nucleation density of electrodeposited Cr is controllable, and the change of nucleation density leads to a large lattice mismatch at the interface, which determines the lattice distortion of the electrodeposited Ni layer. Therefore, it is possible to realize the fragility of the bonding surface by controlling the density of Cr crystal nuclei. It is also possible to control the surface roughness of the demolded surface by controlling the fragility of the interface. For optical mold, surface roughness is the most important assessment index. Surface roughness under different Cr crystal nucleus densities was evaluated. When the Cr crystal nucleus density was  $2.37$ ,  $4.38$ ,  $5.97$ ,  $7.13$ , and  $10.85 \times 10^{11} \text{ cm}^{-2}$ , the roughness was  $R_a = 0.0373 \mu\text{m}$ ,  $R_a = 0.0491 \mu\text{m}$ ,  $R_a = 0.0610 \mu\text{m}$ ,  $R_a = 0.0740 \mu\text{m}$ , and  $R_a = 0.0769 \mu\text{m}$ , respectively. The SEM images are shown in Fig. 9. The surface roughness decreases with the increase of nucleation density.

## 4 Conclusion

In the case of a higher requirement for demolding quality of precision electrodeposition, the control of interface bonding force of electrodeposition is a prominent theme. On the premise that we simply electrodeposited Cr nanocrystalline discrete crystal nuclei, the bonding force between the Cu/Ni interfaces can be adjusted by controlling the density of Cr crystal nuclei. The results of our experiments demonstrate the importance of providing a weak connection at the Cu/Ni interface. This work provides some insights into the proposed concept of Cr nanocrystalline discrete crystal nuclei controlling interface bonding force, which may be crucial for the realization of a new precision electroforming demolding process for metals that can be quantitatively controlled instead of potassium dichromate.



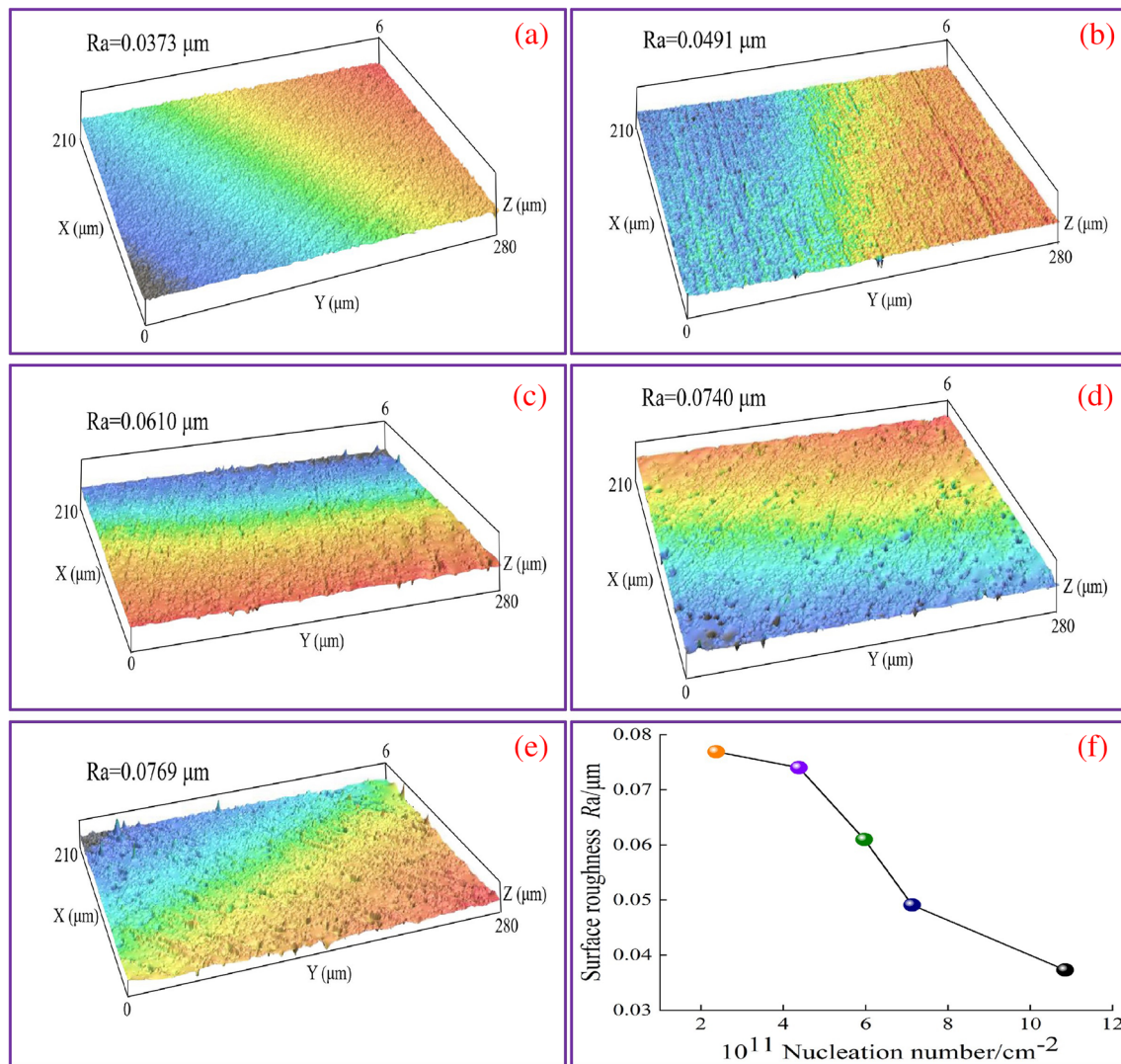


**Fig. 9** Effect of Cr discrete crystal nucleus density on surface roughness. Measured arithmetic means deviation of contour surface roughness  $R_a$  from SEM images (a–e correspond to Cr crystal nucleus den-

sities of  $10.85$ ,  $7.13$ ,  $5.97$ ,  $4.38$ , and  $2.37 \times 10^{11} \text{ cm}^{-2}$ , respectively); **f** effect of Cr discrete nucleus density on surface roughness of Ni deposition layer

**Acknowledgements** This work was supported by the National Natural Science Foundation of China (No. 52175407).

## References

- Roeder M, Guenther T, Zimmermann A (2019) Review on fabrication technologies for optical mold inserts. *Micromachines* 10:233–258. <https://doi.org/10.3390/mi10040233>
- Zhang S, Zhou Y, Zhang H, Xiong Z, To S (2019) Advances in ultra-precision machining of micro-structured functional surfaces and their typical applications. *Int J Mach Tool Manuf* 142:16–41. <https://doi.org/10.1016/j.ijmactools.2019.04.009>
- Barranco A, Borrás A, Gonzalez-Elipe AR, Palmero A (2016) Perspectives on oblique angle deposition of thin films: From fundamentals to devices. *Prog Mater Sci* 76:59–153. <https://doi.org/10.1016/j.pmatsci.2015.06.003>
- Liu CF, Pan CT, Liu KH, Chen YC, Chen JL, Huang JC (2011) Optical Film for LED with Triangular-Pyramidal Array Using Size-Reducible Embossing Method. *J Mater Eng Perform* 20:1544–1553. <https://doi.org/10.1007/s11665-011-9836-0>
- Riemer O (2007) A review on machining of micro-structured optical molds. *Key Eng Mater* 364–366:13–18. <https://doi.org/10.4028/www.scientific.net/KEM.364-366.13>
- Mimura H, Ishikura H, Matsuyama S, Sano Y, Yamauchi K (2011) Electroforming for replicating nanometer-level smooth surface. *J Nanosci Nanotechnol* 11:2886–2889. <https://doi.org/10.1166/jnn.2011.3889>
- Schmidt FJ (1966) Electroforming of large mirrors. *Appl Opt* 5:719–725. <https://doi.org/10.1364/AO.5.000719>
- Lee BK, Cha KJ, Kwon TH (2009) Fabrication of polymer micro/nano-hybrid lens array by microstructured anodic aluminum oxide (AAO) mold. *Microelectron Eng* 86:857–860. <https://doi.org/10.1016/j.mee.2008.11.066>
- Protsenko VS, Danilov FI (2014) Chromium electroplating from trivalent chromium baths as an environmentally

- friendly alternative to hazardous hexavalent chromium baths: comparative study on advantages and disadvantages. *Clean Technol Environ* 16:1201–1206. <https://doi.org/10.1007/s10098-014-0711-1>
10. Peng Z, Gang L, Yangchao T, Xuehong T (2005) The properties of demoulding of Ni and Ni-PTFE moulding inserts. *Sens Actuators A* 118:338–341. <https://doi.org/10.1016/j.sna.2004.01.042>
  11. Smith AM, Watson A, Vaughan DH (1993) The role of oligomeric oxidized species in the deposition rate of chromium from a commercial chromium (III) electrolyte. *Trans IMF* 71(3):106–112. <https://doi.org/10.1080/00202967.1993.11871000>
  12. Kityk AA, Protsenko VS, Danilov FI (2013) Voltammetry study of Cr (III)/Cr (II) system in methanesulfonate and sulfate solutions: Temperature dependences. *Electroanal Chem* 689:269–275. <https://doi.org/10.1016/j.jelechem.2012.10.003>
  13. Dinga WY, Jud DG, Chai WP (2010) The effect of working pressure on the chemical bond structure and hydrophobic properties of PET surface treated by N ion beams bombardment. *Appl Surf Sci* 256:6876–6880. <https://doi.org/10.1016/j.apsusc.2010.04.104>
  14. Ardelean H, Petit S, Laurens P, Marcus P, Arefi-Khonsari F (2005) Effects of different laser and plasma treatments on the interface and adherence between evaporated aluminium and polyethylene terephthalate films: X-ray photoemission, and adhesion studies. *Appl Surf Sci* 243:304–318. <https://doi.org/10.1016/j.apsusc.2004.09.122>
  15. Yang G, Li Y, Pi J, Zhu QQ, Cai JW, Huang ZJ (2019) Control of the adhesion strength between nickel replica and copper mold by electrochemical nucleation of lead. *J Appl Electrochem* 49:1003–1011. <https://doi.org/10.1007/s10800-019-01342-x>
  16. Lai Y, Liu F, Li J, Zhang Z, Liu Y (2010) Nucleation and growth of selenium electrodeposition onto tin oxide electrode. *J Electroanal Chem* 639:187–192. <https://doi.org/10.1016/j.jelechem.2009.11.026>
  17. Molodkina EB, Ehrenburg MR, Broekmann P, Rudnev AV (2020) Electrodeposition of chromium on single-crystal electrodes from solutions of Cr(II) and Cr(III) salts in ionic liquids. *J Electroanal Chem* 860:113892. <https://doi.org/10.1016/j.jelechem.2020.113892>
  18. Eugénio S, Rangel CM, Vilar R, Do Rego AMB (2011) Electrodeposition of black chromium spectrally selective coatings from a Cr(III)-ionic liquid solution. *Thin Solid Films* 519:1845–1850. <https://doi.org/10.1016/j.tsf.2010.10.029>
  19. Protsenko VS, Danilov FI, Gordiienko VO, Kwon SC, Kim M, Lee JY (2011) Electrodeposition of hard nanocrystalline chrome from aqueous sulfate trivalent chromium bath. *Thin Solid Films* 520:380–383. <https://doi.org/10.1016/j.tsf.2011.07.036>
  20. Grujicic D, Pesic B (2002) Electrodeposition of copper: the nucleation mechanisms. *Electrochim Acta* 47(18):2901–2912. [https://doi.org/10.1016/S0013-4686\(02\)00161-5](https://doi.org/10.1016/S0013-4686(02)00161-5)
  21. Aguirre MDC (2019) Nucleation and growth mechanisms of palladium, nanoflower-shaped, and its performance as electrocatalyst in the reduction of Cr(VI). *J Appl Electrochem* 49:795–809. <https://doi.org/10.1007/s10800-019-01323-0>
  22. Scharifker B, Hills G (1983) Theoretical and experimental studies of multiple nucleation. *Electrochim Acta* 28:879–889. [https://doi.org/10.1016/0013-4686\(83\)85163-9](https://doi.org/10.1016/0013-4686(83)85163-9)
  23. Song YB, Chin DT (2002) Current efficiency and polarization behavior of trivalent chromium electrodeposition process. *Electrochim Acta* 48:349–356. [https://doi.org/10.1016/S0013-4686\(02\)00678-3](https://doi.org/10.1016/S0013-4686(02)00678-3)
  24. Zhao H (2020) Mechanism of chromium electrodeposition from Cr(III) baths on nickel and chromium electrode surfaces. *Int J Electrochem Sci* 15(2020):8979–8989. <https://doi.org/10.20964/2020.09.23>
  25. Radisic A, Vereecken PM, Hannon JB, Searson PC, Ross FM (2006) Quantifying electrochemical nucleation and growth of nanoscale clusters using real-time kinetic data. *Nano Lett* 6:238–242. <https://doi.org/10.1021/nl052175>
  26. Sajjadnejad M, Omidvar H, Javanbakht M, Mozafari A (2017) Textural and structural evolution of pulse electrodeposited Ni/diamond nanocomposite coatings. *J Alloy Compd* 704:809–817. <https://doi.org/10.1016/j.jallcom.2016.12.318>
  27. Xue Z, Lei W, Wang Y, Qian H, Li Q (2017) Effect of pulse duty cycle on mechanical properties and microstructure of nickel-graphene composite coating produced by pulse electrodeposition under supercritical carbon dioxide. *Surf Coat Technol* 325:417–428. <https://doi.org/10.1016/j.surfcoat.2017.07.017>
  28. Rashidi AM, Amadeh A (2010) Effect of electroplating parameters on microstructure of nanocrystalline nickel coatings. *J Mater Sci Technol* 26:82–86. [https://doi.org/10.1016/S1005-0302\(10\)60013-8](https://doi.org/10.1016/S1005-0302(10)60013-8)
  29. Sarac U, Baykul MC (2013) Morphological and microstructural properties of two-phase Ni–Cu films electrodeposited at different electrolyte temperatures. *J Alloy Compd* 552:195–201. <https://doi.org/10.1016/j.jallcom.2012.10.071>
  30. Haciismailoglu M, Alper M (2011) Effect of electrolyte pH and Cu concentration on microstructure of electrodeposited Ni-Cu alloy films. *Surf Coat Tech* 206:1430–1438. <https://doi.org/10.1016/j.surfcoat.2011.09.010>
  31. Nasirpour F, Sanaeian MR, Samardak AS, Sukovatitsina EV, Ognev AV, Chebotkevich LA, Hosseini MG, Abdolmaleki M (2014) An investigation on the effect of surface morphology and crystalline texture on corrosion behavior, structural and magnetic properties of electrodeposited nanocrystalline nickel films. *Appl Surf Sci* 292:795–805. <https://doi.org/10.1016/j.apsusc.2013.12.053>
  32. Helmersson U, Johansson BO, Sundgren JÅE, Hentzell HTG, Billgren P (1998) Adhesion of titanium nitride coatings on high-speed steels. *J Vac Sci Technol A* 3(1998):308–315. <https://doi.org/10.1116/1.573256>
  33. Lin Z, Bristowe PD (2007) Microscopic characteristics of the Ag(111)/ZnO(0001) interface present in optical coatings. *Phys Rev B* 75:205423–205435. <https://doi.org/10.1103/PhysRevB.75.205423>
  34. Weng S, Chen X, Yue X, Fu T, Peng X (2019) Inapparent strengthening effect of twin interface in Cu/Pd multilayered films with a large lattice mismatch. *J Nanomater* 9:1778–1791. <https://doi.org/10.3390/nano9121778>
  35. Wu CD, Huang BX, Li HX (2020) Effects of interfacial defect on deformation and mechanical properties of Cu/Ni bilayer—a molecular dynamics study. *Thin Solid Films* 707:138050–138056. <https://doi.org/10.1016/j.tsf.2020.138050>
  36. Unger WES, Lippitz A, Gross TH, Friedrich JF, Wöll Ch, Nick L (1999) The use of octadecyltrichlorosilane self-assembled layers as a model for the assessment of plasma treatment and metallization effects on polyolefins. *Langmuir* 15:1161–1166. <https://doi.org/10.1021/la981174l>
  37. Chen SD, Zhou YK, Soh AK (2012) Molecular dynamics simulations of mechanical properties for Cu(001)/Ni(001) twist boundaries. *Comput Mater Sci* 61:239–242. <https://doi.org/10.1016/j.commatsci.2012.04.035>
  38. Weng S, Ning H, Hu N, Yan C, Fu T, Peng X, Fu S, Zhang J, Xu C, Sun D, Liu Y, Wu L (2016) Strengthening effects of twin interface in Cu/Ni multilayer thin films—a molecular dynamics study. *Mater Des* 111:1–8. <https://doi.org/10.1016/j.matdes.2016.08.069>
  39. Fu T, Peng X, Chen X, Weng S, Hu N, Li Q, Wang Z (2016) Molecular dynamics simulation of nanoindentation on Cu/Ni nanotwinned multilayer films using a spherical indenter. *Sci Rep* 6:35665. <https://doi.org/10.1038/srep35665>
  40. Zhu XY, Liu XJ, Zong RL, Zeng F, Pan F (2010) Microstructure and mechanical properties of nanoscale Cu/Ni multilayers. *Mat Sci Eng A* 527:1243–1248. <https://doi.org/10.1016/j.msea.2009.09.058>

**Publisher's note** Springer Nature remains neutral with regard to jurisdictional claims in published maps and institutional affiliations.